

INFLUENCE OF AN ACTIVE GURNEY FLAP UPON THE AERODYNAMIC AND PERFORMANCE PROPERTIES OF A MAIN ROTOR IN VARIOUS STATES OF HELICOPTER FLIGHT

Wieczyslaw Stalewski, Institute of Aviation, Warsaw, Poland

Abstract

In rotorcraft engineering the Active Gurney Flap (AGF) is a small tab located at lower surface of the blade near its trailing edge. The tab is oscillating perpendicularly to the blade surface. When deployed it deflects air stream behind the blade trailing edge downwards, leading to the lift increase. On the advancing blade, the AGF is retracted to minimise rotor torque. The AGF technology may improve the overall performance of a helicopter. However, to take full advantage of such potential benefits, it is necessary to gain knowledge about physical phenomena related to the AGF. This especially concerns determination of states of helicopter flight, in which the application of the AGF technology could be the most beneficial. Explaining such the problems was the main subject of the research presented in the paper. Computational simulations of the investigated phenomena have been conducted using the URANS solver. To simulate a motion of the AGF mounted on the rotor blades, the original methodology, based on computational-mesh-deformation approach has been developed and implemented. The presented computational results have concerned mainly simulations of full scale main rotor with blades equipped with the AGFs. Additionally, some quasi-two-dimensional studies, conducted in conditions similar as in a real flight, have been discussed too. The overall conclusion from the conducted computational studies is, that the greatest benefits of using the AGF technology on the rotor blades may be expected in states of helicopter flight characterised by higher values of the rotor thrust coefficient, especially when the retreating-blade dynamic stall occurs.

1. INTRODUCTION

There are several general approaches concerning introduction of very promising active-flow-control technology on blades of helicopter main rotor. The first, mostly investigated, utilises mechanical devices, dynamically activated and inactivated during rotor-rotation cycles. The alternative approaches may be based on fluidic or even plasmatic devices. The solution presented in this paper represents the mechanical approach and is based on the idea of micro device named the Gurney flap.

The classic Gurney flap^[9] is a small, flat tab located at a pressure side of lifting surface near its trailing edge. The tab deflects the air stream behind the trailing edge downwards, leading to lift increase. Solutions based on the Gurney-flap idea are applied in many areas. In helicopter rotor applications, instead of static tab, the dynamically deployed Active Gurney Flap (AGF) is taken into consideration. The originally patented AGF^[2] is a small tab located at lower surface of the blade near its trailing edge, oscillating perpendicularly to the blade surface. When deployed (usually on the azimuthal positions corresponding to the retreating blade), the tab deflects air stream behind the blade trailing edge downwards, leading to the lift increase. On the advancing blade, the AGF is retracted to minimise rotor torque. It is expected that AGF may improve a performance of helicopter. However, to take full advantage of such potential benefits, it is

necessary to gain knowledge about physical phenomena related to the AGF and to answer the question: in which states of helicopter flight, the application of AGF may to be the most beneficial from point of view of improvement of helicopter performance? The answer to this question was one of the main purposes of the research presented in this paper.

The computational studies on the AGF technology implemented on blades of helicopter main rotor, have been conducted within the EU 7th FWP Project COMROTAG^{[7],[8]}, titled: "Development and Testing of Computational Methods to Simulate Helicopter Rotors with Active Gurney Flap".

The paper summarises results of the COMROTAG project. Therefore it focuses on overall evaluation of expected helicopter-performance benefits resulting from application of the AGF on the rotor blades. Special attention is paid for a determination of helicopter-flight states in which such benefits are the most evident. Additionally, based on conducted computational simulations, the physical phenomena leading to these benefits are tried to be explained.

2. METHODOLOGY

A flight of main rotor with blades equipped with the AGF have been simulated based on computational methodology schematically presented Figure 1.

The flight simulation consists in the solution of Unsteady Reynolds Averaged Navier-Stokes

Equations (URANS) in the domain surrounding the rotating rotor. The URANS equations are solved using the ANSYS FLUENT^[1] code. All specific rotorcraft computations are realised by developed in-house UDF module Virtual-Rotor-3D^{[7],[8]}. This module is responsible for modelling of rotation of the rotor, blade feathering and flap-and-lag motion as well as cyclic motion of the AGF. The structure of computational mesh is shown in Figure 2. The mesh is divided into several sub domains. Around each blade, the cylinder-conical volume zone is defined. Such zones are embedded in a cylinder-volume zone which is embedded in a far-field modelling zone. During the rotor flight simulation, the mesh surrounding each blade is moving together with the blade. This motion is a combination of feathering, flapping and lead-lag motion. Additionally the mesh

surrounding each blade is rotating together with the cylindrical zone, around the rotor-rotation axis. The motion of meshes surrounding the blades, relative to the cylindrical zone, is realised by the use of Dynamic Mesh and Sliding Mesh techniques implemented in the ANSYS FLUENT solver. The rotational motion of the cylindrical zone inside the far-field zone is realised in the same way. The mesh inside a separate volume zone surrounding the AGF is locally deformed so as to model the AGF motion, as shown in Figure 3. The developed, original method of the AGF motion ensures high quality of deformed mesh as well as full repeatability of deformations. The method seems to be competitive alternative to the Overlapping Grid Methods^[5], usually used to model the flow around the AGF.

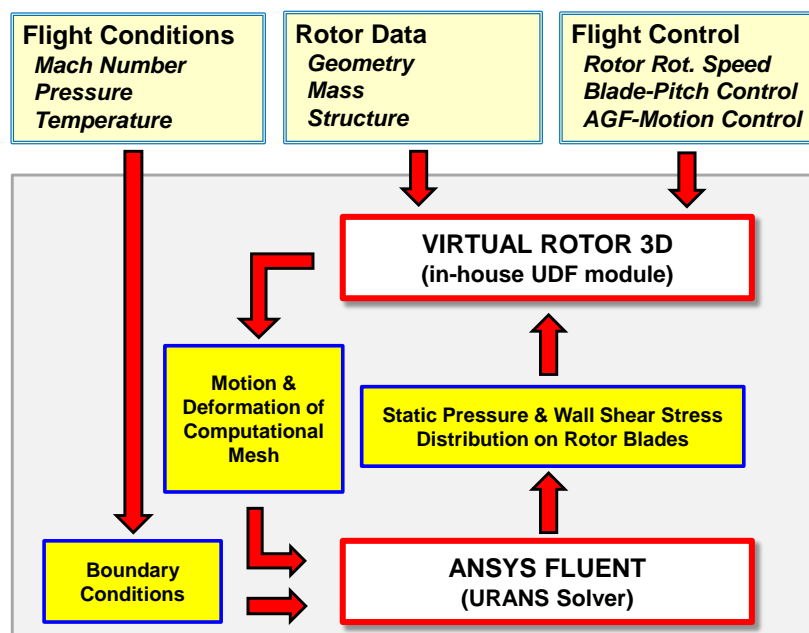


Figure 1. The general scheme of developed methodology of simulation of flight of helicopter main rotor with blades equipped with AGF.

Coupled equations of flap and lead-lag motion of the blades are solved simultaneously with the solution of URANS equations, taking into account effects of dampers and springs (or elastomeric bearing), if any. The flap-and-lag motion is described by the system of four ordinary differential equations of the first order. There are four unknown functions in this system: $\beta(t)$, $\zeta(t)$, $\dot{\beta}(t)$, $\dot{\zeta}(t)$, where β is the blade-flap angle, ζ is the blade-lag angle, $\dot{\beta} = d\beta/dt$, $\dot{\zeta} = d\zeta/dt$. The system of ordinary differential equations is solved separately for each blade, using explicit, three-step Adams–Bashforth method^[3].

The blade collective-and-cyclic-pitch controls may be changed during the simulation which is used when trimming the rotor, i.e. establishing the blade pitch controls so as to obtain required thrust as well as pitching and rolling moments of the rotor.

The developed code Virtual-Rotor-3D has been partially validated, in case of forward flight of model rotor. Due to lack of experimental results concerning dynamically deployed AGF, the CFD and WTT^[4] results were compared with each other, in respect to the Clean-Blade and Passive-Gurney-Flap configurations, configurations, corresponding to fixed Gurney flaps fully retracted and fully deployed, respectively. As it is shown in Figure 4 the CFD and WTT results are converging quite well.

The developed methodology has been additionally adapted for solving simplified 2D and 2.5D cases. The later approach has been validated in respect to the experimental investigations of blade segment equipped with oscillating AGF^{[7],[8]}. Good convergence of computational and experimental results, concerns both the time variable global

aerodynamic coefficients (Figure 5) and unsteady-vortex-shedding phenomenon (Figure 6), in case of WTT results captured using the PIV technique.

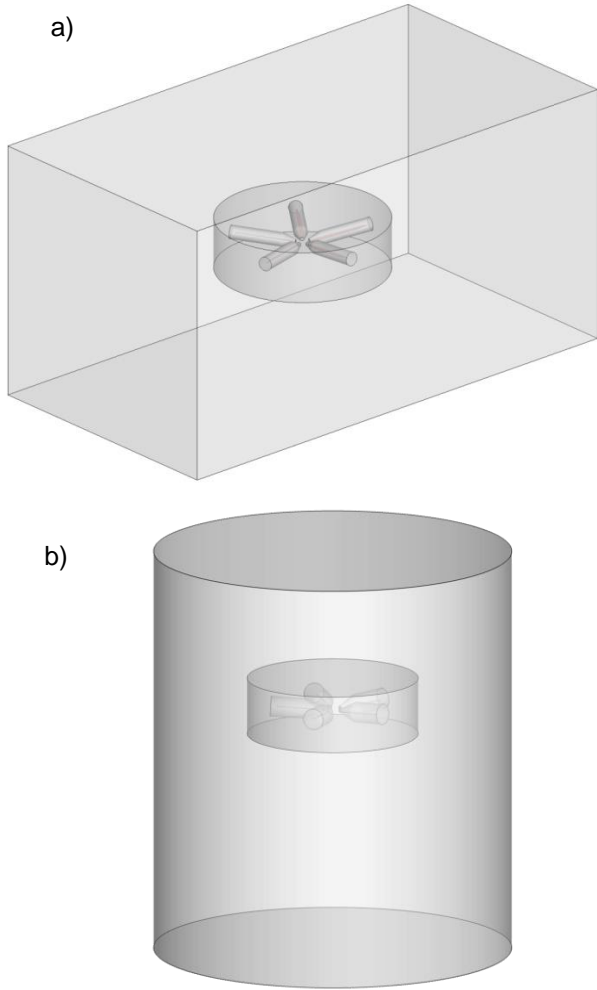


Figure 2. Structure of computational mesh intended for computational simulations of: a) forward-flight, b) hover of helicopter main rotor.

3. 2.5-DIMENSIONAL STUDY ON ACTIVE GURNEY FLAP

A simplified, 2.5D study has been conducted, mainly to analyse the physical phenomena occurring in the flow around the rotor-blade segment equipped with oscillating AGF. The conducted computational simulations have corresponded to the experimental research, focused on the blade segment of chord 0.4 m placed in the test chamber of wind tunnel, as shown in Figure 7. The blade segment was investigated in oscillatory motion consisting in harmonic changes of its angle of attack. Simultaneously, the AGF was cyclically deployed and retracted. General schedule of motion of both the blade segment and the AGF, is shown in Figure 8. The CFD simulations have been conducted for the free-stream flow conditions: $M=0.3$ and $Re =$

$2.8 \cdot 10^6$. Two cases of oscillatory motion of the blade segment have been taken into consideration. In terms of range of angle of attack (α) and oscillation frequency (f_α) these cases may be described as follows:

- Case 1: $\alpha = 8^\circ \pm 6^\circ$, $f_\alpha=3\text{Hz}$;
- Case 2: $\alpha = 14^\circ \pm 6^\circ$, $f_\alpha=7\text{Hz}$;

For both these cases, two configurations have been investigated: reference configuration with AGF fully retracted and configuration with moving AGF, according to the ramp kinematics shown in Figure 8.

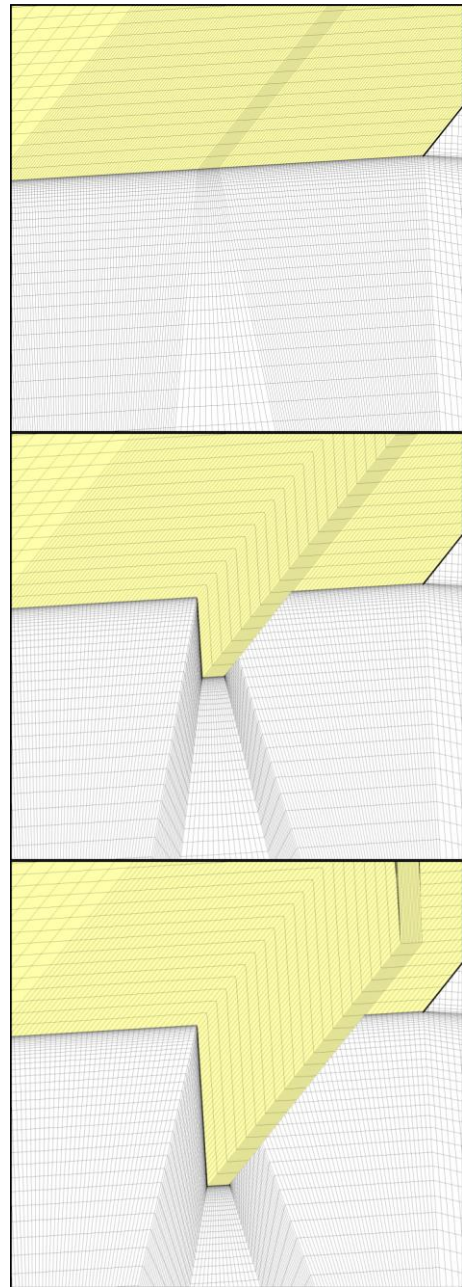


Figure 3. Sequential stages of 3D-mesh deformations during the deployment of the AGF.

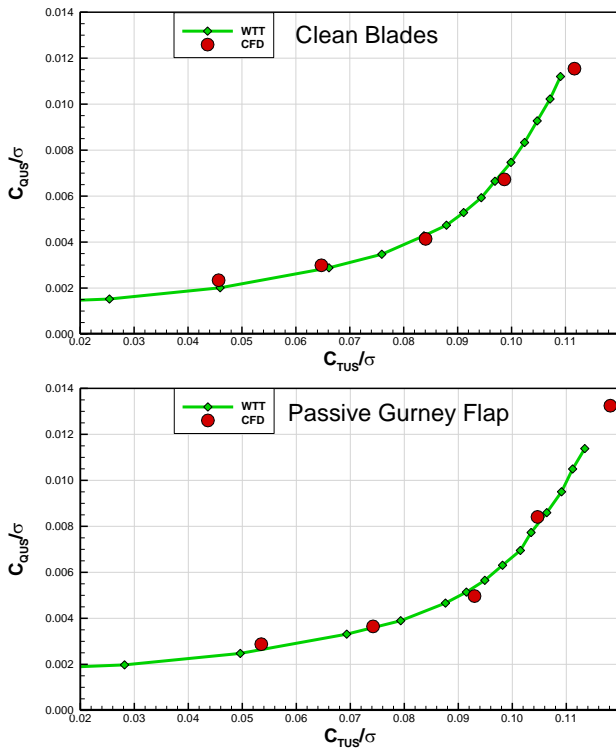


Figure 4. Torque Coefficient (C_{QUS}/σ) vs. Thrust Coefficient (C_{TUS}/σ). Forward flight of Model Rotor. Comparison of results of CFD and WTT [3]. Configurations: top: Clean-Blades, bottom: Passive Gurney Flap.

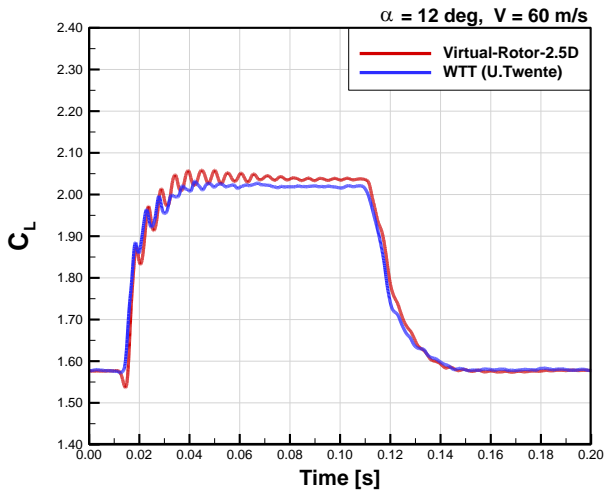


Figure 5. Changes of lift coefficient (C_L) during one period of AGF deployment-retraction cycle. Comparison of CFD and WTT (University of Twente) results.

Results of CFD simulations conducted for the flow conditions "Case 1" are presented in Figure 9 and Figure 10. In these figures "Dynamic Baseline 1" refers to reference configuration (clean blade) while "Dynamic AGF 1" refers to the configuration with moving AGF. In discussed case of flow conditions, the strong dynamic stall did not occur (which was also confirmed through analysis of transient skin-

friction-coefficient distributions). As shown in Figure 9, in the case of "Dynamic AGF 1" configuration, the deployment of Gurney flap at higher angles of attack, compared to the reference configuration "Dynamic Baseline 1", leads to increase of maximum lift coefficient of about 0.35 and to decrease of aerodynamic efficiency (C_L/C_D) for the same value of lift coefficient (C_L), except the highest values of C_L , unreachable for the reference configuration.

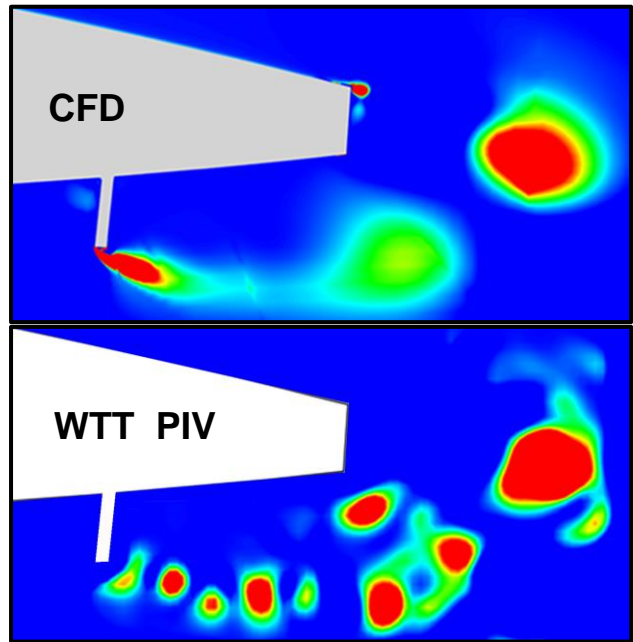


Figure 6. Visualisation of vortex-shedding phenomenon. Q-criterion contours at a moment of fully deployed AGF. Comparison of results of CFD (top) and WTT (bottom).

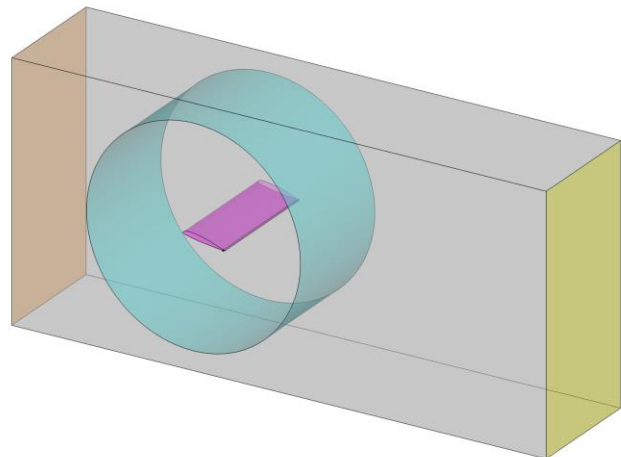


Figure 7. Computational model of the blade segment equipped with the AGF, investigated in the test chamber of wind tunnel.

Presented in Figure 10 results of frequency-domain analysis of pitching moment coefficient (C_m) made for the "Dynamic AGF 1" configuration indicated two dominant frequencies: 1118.9 Hz and 3016.7 Hz.

The former frequency was close to the vortex-shedding dominant frequency captured in the static-case simulation for fully deployed Gurney flap. The later frequency was close to the dominant frequency observed in the static-case simulation for fully retracted Gurney flap. Results of frequency-domain analysis of pitching moment coefficient (C_m) made for the "Dynamic Baseline 1" configuration indicated one dominant frequency: 3015.0 Hz which is close to the dominant frequency measured in the static-case simulation for the Gurney flap fully retracted.

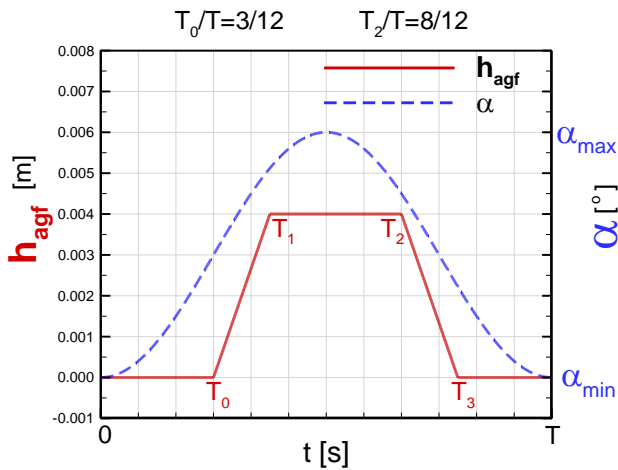


Figure 8. Assumed changes of angle of attack (α) and height of AGF (h_{agf}) during one period of oscillatory motion of the blade segment equipped with the AGF.

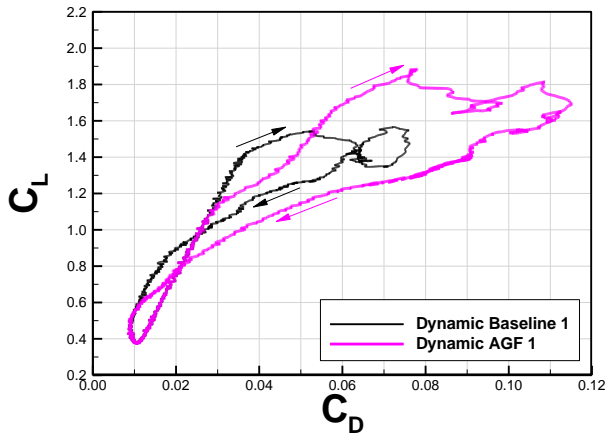


Figure 9. Dependency: lift coefficient (C_L) vs. drag coefficient (C_D) during one cycle of oscillatory motion of the blade segment, with frequency 3Hz. Comparison of results obtained for "Dynamic Baseline 1" and "Dynamic AGF 1" configurations.

Results of CFD simulations conducted for the "Case 2" of flow conditions are presented in Figure 11 and Figure 12. In these figures "Dynamic Baseline 8" refers to reference configuration (clean blade segment) while "Dynamic AGF 9" refers to the configuration with moving AGF. Generally, it may be concluded, that the discussed conditions favour the strong dynamic stall at the highest angles of attack.

It concerns the both considered configurations and it was confirmed through flow visualisations as well as through analysis of transient skin-friction-coefficient distributions. Both configurations reach the maximum lift in the dynamic-stall state of the flow. In the case of "Dynamic AGF 9" configuration, the deployment of the Gurney flap at higher angles of attack, led to increase of maximum lift coefficient of about 0.3 compared to the reference configuration.

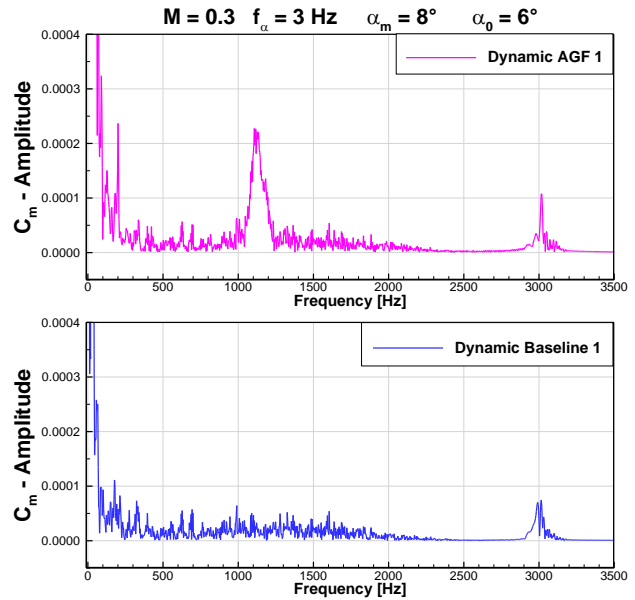


Figure 10. Frequency-domain analysis of pitching moment coefficient (C_m) in case of oscillatory motion of the blade segment, with frequency 3 Hz. Comparison of results obtained for "Dynamic Baseline 1" and "Dynamic AGF 1" configurations.

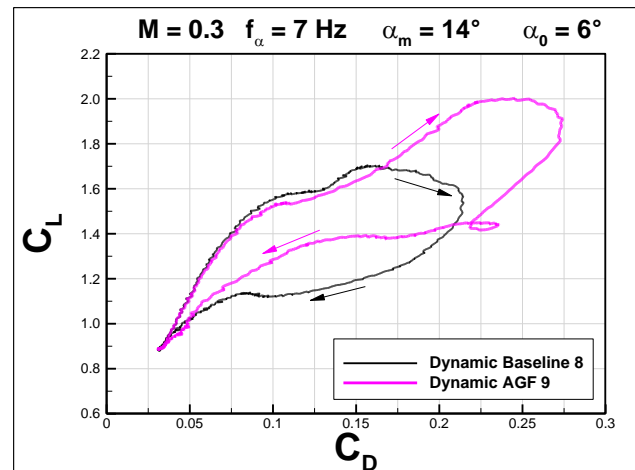


Figure 11. Dependency: lift coefficient (C_L) vs. drag coefficient (C_D) during one cycle of oscillatory motion of the blade segment, with frequency 3Hz. Comparison of results obtained for "Dynamic Baseline 8" and "Dynamic AGF 9" configurations.

Compared to the reference configuration, the "Dynamic AGF 9" configuration in a phase of growing AoA, indicated just slightly lower aerodynamic efficiency (C_L/C_D) for the same values of lift coefficient (C_L), except the highest values of C_L , unreachable for the reference configuration. However, at the dropping phase of AoA and for $C_L < 1.4$, a considerably increased aerodynamic efficiency has been observed for the configuration with moving AGF. In the discussed flow conditions, the strong unsteady vortex shedding did not occur. However weaker, high-frequency oscillations of pitching-moment coefficient were visible in obtained results. This confirmed presence of weak vortex shedding in the discussed cases. Especially, it concerns the "Dynamic AGF 9" configuration, for which the unsteady vortex shedding has been confirmed through vorticity visualisations.

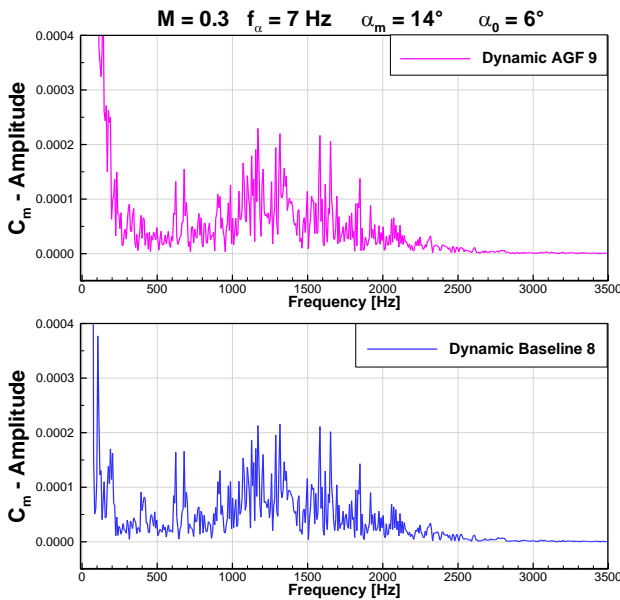


Figure 12. Frequency-domain analysis of pitching moment coefficient (C_m) in case of oscillatory motion of the blade segment, with frequency 7 Hz. Comparison of results obtained for "Dynamic Baseline 8" and "Dynamic AGF 9" configurations.

Described differences in physical phenomena observed in the "Case 1" and "Case 2" of flow conditions are explained partially in Figure 13. The figure presents the comparison of contours of flow vorticity component perpendicular to the plane of symmetry of the blade segment, for the fully attached flow to the blade surface (observed in "Case 1") and for the flow strongly detached on the upper surface of the blade (observed in "Case 2"). In this figure, the clockwise rotating vortices are marked in warm colours, while cold colours are related to counter clockwise rotating vortices. In the "Case 1", the flow is fully attached to the blade surface. On the upper and lower surfaces, the counter rotating vortices are flowing to the trailing

edge. When reaching the trailing edge, they influence strongly on each other, which leads to unsteady phenomenon called the Kármán vortex street. As a result of this phenomenon, strong oscillation of pressure and global aerodynamic characteristics are observed. For the "Case 2" of flow conditions, the flow is detached on the upper surface of the blade. As a result, the flow vorticity is fuzzy in this region. When reaching the trailing edge, the strong vortices flowing along the lower surface, do not meet counter rotating vortices flowing from the upper surface. This asymmetry is the reason why the unsteady vortex shedding is much weaker in this case.

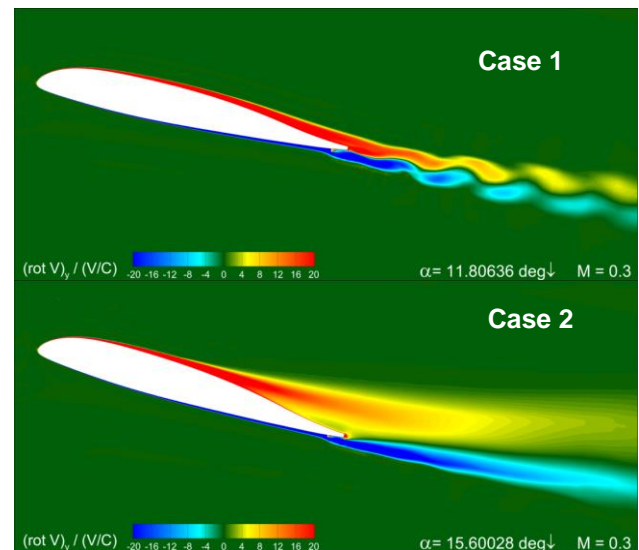


Figure 13. Comparison of contours of vorticity component perpendicular to the plane of symmetry of the blade segment, for the flow fully attached to the blade surface (Case 1) and for the flow strongly separated on the upper surface of the blade (Case 2).

The "Case 2" represents such type of flow conditions, in which application of AGF gives some benefits in respect to the aerodynamic efficiency. On the other hand, in flow conditions represented by the "Case 1", the clean-blade configuration is more favourable. This phenomenon may be partially explained by the different types of flow on the upper surface of the blade in the both compared cases. In the "Case 1" the flow is fully attached, even at higher angles of attack. In such conditions the drag of clean blade segment is relatively small. Deployment of the AGF in such conditions causes significant relative growth of the drag force, which cannot be compensated by simultaneous growth of the lift force. As a result, the decrease of aerodynamic efficiency is observed for the configuration with fully deployed AGF. In the "Case 2" of flow conditions, the significant flow separation appears at higher angles of attack. In such conditions the increase of drag force being a result of the AGF deployment is

relatively small, compared to the significant overall drag of the clean blade, typical for the strongly separated flows. Additionally, the dynamic-stall phenomenon usually leads to momentary increase of lift force. Both of these phenomena together lead to the observed growth of an aerodynamic efficiency of the blade segment equipped with moving AGF.

4. COMPUTATIONAL SIMULATIONS OF FORWARD FLIGHT OF MODEL ROTOR

Three-dimensional, computational studies on flow control on rotor blades via AGF, have been conducted for the case of 4-blade, fully articulated model rotor of radius 1.1m. Its rectangular blades of chord 0.09m were equipped with AGF in spanwise position from 53.5% to 68.5% of rotor radius. The maximum deployment of the AGF was approximately 2.8% of blade chord. The computational tests were conducted for two reference configurations: 1) rotor with Clean Blades, 2) rotor with blades equipped with fixed, Passive Gurney Flaps (PGF). Two configurations with moving AGF have been taken into consideration. They have differing from each other in presented in Figure 14 two types of AGF motion: sinusoidal and ramp.

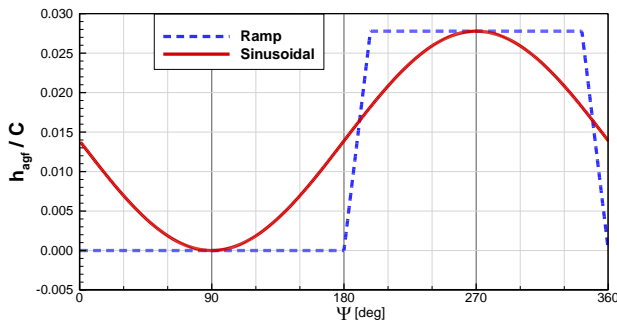


Figure 14. Variants of AGF-motion schedules, considered in simulations of flight of model rotor.

Simulations of flight of the model rotor have been conducted for a flight velocity 48 m/s, rotor rotational speed 1600 rpm and ISA-Sea-Level atmospheric conditions. For each rotor configuration, the simulations have been conducted for selected angles of collective pitch of the rotor blades. In the each single simulation, the components of the blade cyclic pitch were established so as to zero the first harmonics of blade flapping.

Figure 15 shows that even fixed Gurney flap (PGF) implemented on the rotor blades, gave some performance benefits, i.e. lower torque coefficient for the same thrust coefficient, in comparison to the "Clean Blades" configuration. However, these benefits were visible only above certain level of the thrust coefficient (approximately for $C_{TUS}/\sigma > 0.084$).

Analysing presented in Figure 15 results for the configuration AGF(sinusoidal), it may be concluded, that for higher values of thrust, this configuration indicated similar performance benefits as PGF configuration. For lower values of thrust the AGF(sinusoidal) configuration did not indicate such significant power penalty, which was observed for the PGF configuration. The above conclusions concern also the AGF(ramp) configuration, which is confirmed by the graphs presented Figure 16.

For a more clear assessment of potential benefits or losses in helicopter performance as a result of application of AGF on the rotor blades, a "power reduction" coefficient (ΔP) has been introduced. This coefficient, for a given rotor thrust, is defined as follows:

$$(1) \quad \Delta P = \frac{P_{ref} - P}{P_{ref}}$$

where P is the power required to generate given thrust by the rotor, while P_{ref} is the power required to generate the same thrust by the rotor equipped with clean blades.

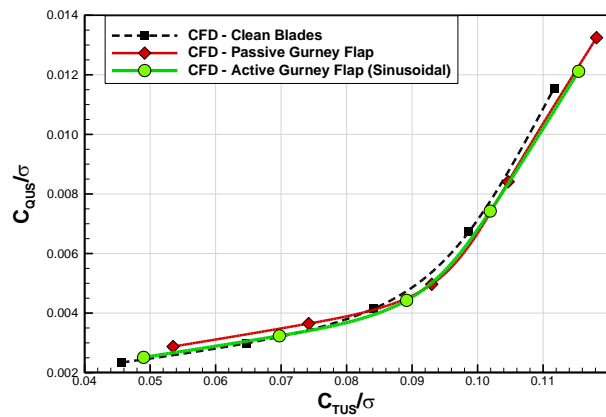


Figure 15. Forward flight of Model Rotor. Comparison of dependences (C_{QUS}/σ) vs. (C_{TUS}/σ) obtained for Clean-Blades, PGF and AGF(Sinusoidal) configurations.

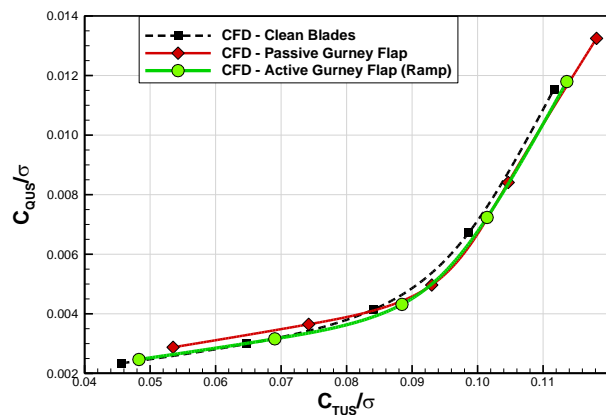


Figure 16. Forward flight of Model Rotor. Comparison of dependences (C_{QUS}/σ) vs. (C_{TUS}/σ) obtained for Clean-Blades, PGF and AGF(Ramp) configurations.

The analysis of the graphs presented in Figure 17 leads to the following conclusions:

- For higher values of thrust coefficient, where the probability of dynamic-stall appearance on the retreating blade increases, the configurations: "AGF-Sinusoidal" and "AGF-Ramp" show some favourable, positive values of power-reduction coefficient (ΔP), similar to those that are achieved by the "PGF" configuration. Maximum values of ΔP are 6.7%, 7.1% and 6.8%, respectively for "AGF-Sinusoidal", "AGF-Ramp" and "PGF" configurations.
- For lower values of thrust coefficient, the configurations: "AGF-Sinusoidal" and "AGF-Ramp" indicate only slightly negative values of ΔP as opposed to the "PGF" configuration for which unfavourable negative coefficient ΔP exceeds -10%. This means more than 10% increase in power required to generate the same thrust, relative to the smooth blade configuration.
- The "AGF-Ramp" configuration seems to be slightly more favourable in terms of helicopter-performance improvement than the "AGF-Sinusoidal" configuration

5. COMPUTATIONAL STUDIES ON THE AGF TECHNOLOGY IMPLEMENTED ON A REAL-SCALE MAIN ROTOR

The final stage of the COMROTAG project concerned the computational studies on the AGF technology implemented on a real-scale main rotor of the helicopter. The subject of these investigations was the 5-blade main rotor presented in Figure 18.

5.1. Computational Studies on the Active Gurney Flap in Forward Flight of Real-Scale Main Rotor

The main goal of conducted simulations of forward flight of real-scale main rotor, was to estimate potential benefits of application of the AGF technology in conditions of real flight of the helicopter. Therefore, in each considered flight priority, the simulations were conducted twice, for the rotor blades equipped with moving AGFs according to the sinusoidal kinematics and for the reference configuration - a rotor with clean blades. For both these configurations efforts were made to achieve the same thrust as well pitching and rolling moments generated by the rotor. This should have been achieved through the use of rotor trimming procedure, consisting in establishing the controls of blade collective and cyclic pitch, so as to obtain required thrust and moments generated by the rotor. However, the rotor trimming was carried out only with certain accuracy. Therefore, to assess potential benefits of AGF application, the factor called the

Power Loading and denoted by PL [6] was proposed to compare the efficiency of different helicopter main rotors. The Power Loading has been defined as a ratio: thrust (T) to power (P):

$$(2) \quad PL = T / P$$

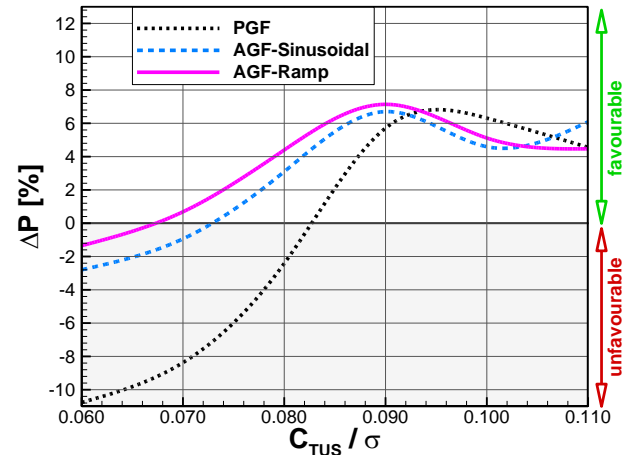


Figure 17. Dependency of power-reduction coefficient (ΔP) vs thrust coefficient (C_{TUS}) related to rotor solidity (σ) evaluated for PGF, AGF(Sinusoidal) and AGF(Ramp) configurations.

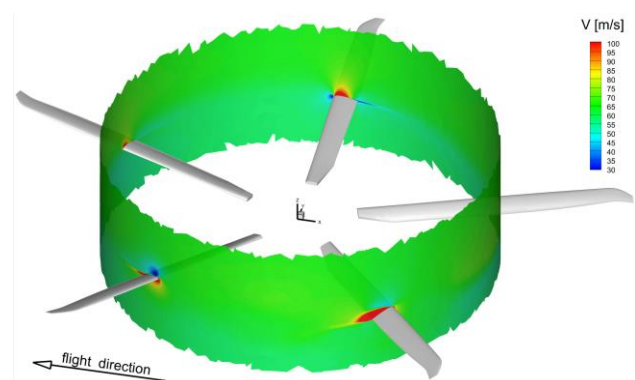


Figure 18. Simulation of forward flight of five-blade, real-scale main rotor with blades equipped with the AGFs. Velocity-magnitude contours around the rotor blades.

The helicopter-forward-flight simulations have been conducted for several flight priorities, differing in altitude, velocity and thrust generated by the rotor. For the most promising flight Priority No. 1, the rotor with implemented AGF-technology achieved the 7.3% increase of PL, compared to the reference configuration. If this impressive result were confirmed in flight tests, it would prove considerable improvement of helicopter performance in fast-forward-flight conditions.

In the mentioned above simulation of the most promising flight Priority No. 1, the helicopter main rotor was flying at a speed of 84.2 m/s at altitude 3413 m. The required rotor thrust coefficient was $C_{TUS}=0.01085$. After trimming the rotor so as to

obtain required thrust and moments, it turned out that in the considered flight conditions, the dynamic-stall phenomenon occurred on the retreating blade. This phenomenon is visualised in Figure 19, for both configurations: "AGF-Sinusoidal" (with moving AGF) and "Clean Blades" by the use of iso-surfaces of Q-criterion. For the configuration "AGF-Sinusoidal" the same phenomenon, in terms of vorticity-magnitude contours, is presented in Figure 20.

To better understand the reason for the significant increase in PL by using of the AGF-technology in the discussed Priority No. 1 of helicopter-flight conditions, it is worthwhile to analyse in such conditions the kinematic and aerodynamic parameters of a single blade as functions of its azimuthal position. Figure 21 presents the blade pitch angle (θ) as a function of the blade azimuthal position (Ψ), in trimmed state of the rotor, for the flight Priority No. 1. Computational results obtained for the "AGF-Sinusoidal" and "Clean Blades" configurations are compared to each other. Presented graphs show, that the minimum blade

pitch is the same for both compared configurations. However, the maximum blade pitch is by 1 degree lower for the "AGF-Sinusoidal" configuration. This means, that rotor with blades equipped with moving AGFs needed slightly lower maximum commanded pitch of the blades, to achieve the trimmed state described by the required thrust and moments.

Graphs compared in Figure 22 show that in fact, for both configurations the same required thrust has been achieved. The figure presents the single-blade thrust coefficient ($C_{TUS(b)}$) as a function of the blade azimuthal position (Ψ). Graphs corresponding to "AGF-Sinusoidal" and "Clean Blades" configuration are very close to each other. The same concerns the averaged values of the rotor thrust as well as pitching and rolling moments generated by the rotor. However in respect to the single-blade torque coefficient ($C_{QUS(b)}$) as a function of the blade azimuthal position (Ψ) the differences between "AGF-Sinusoidal" and "Clean Blades" configuration are evident, which is shown in Figure 23.

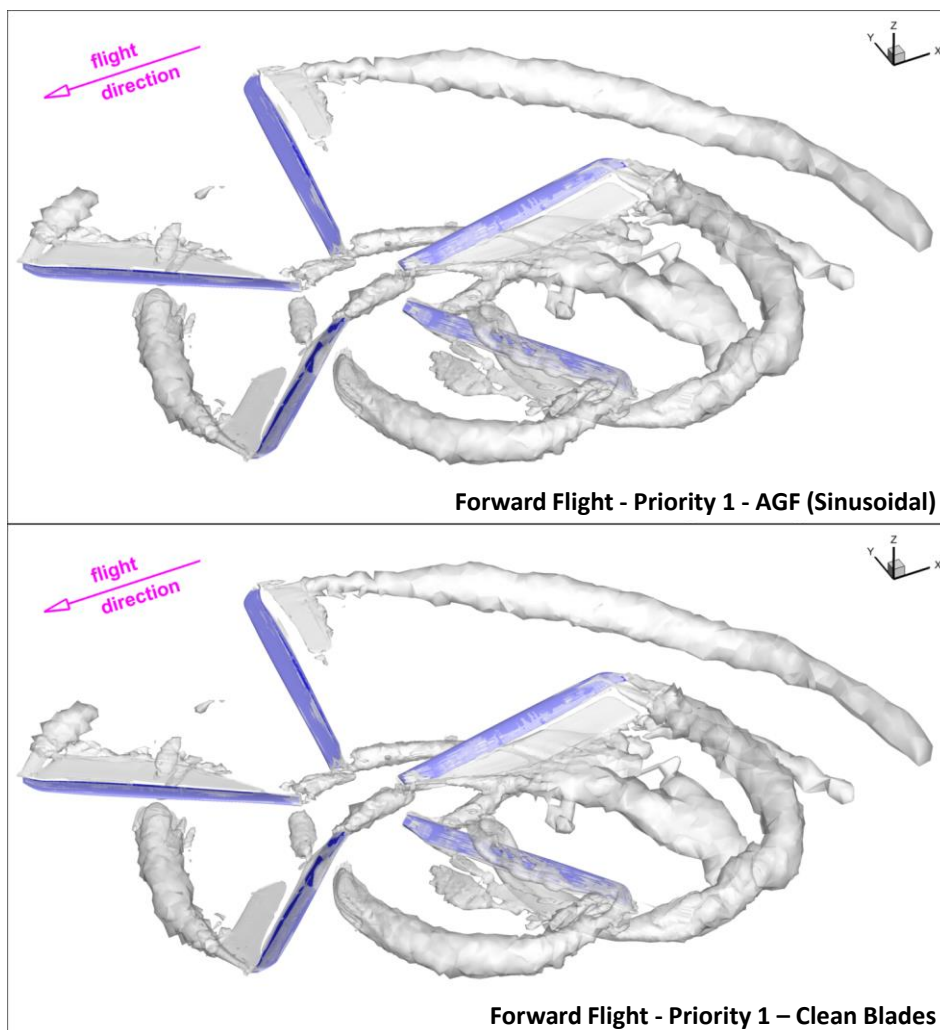


Figure 19. Izo-surfaces of Q-Criterion ($Q_c/\Omega_R^2 = 0.25$) visualising vortex structures generated in forward flight Priority No. 1, for two configurations of rotor blades: "AGF(Sinusoidal)" and "Clean Blades".

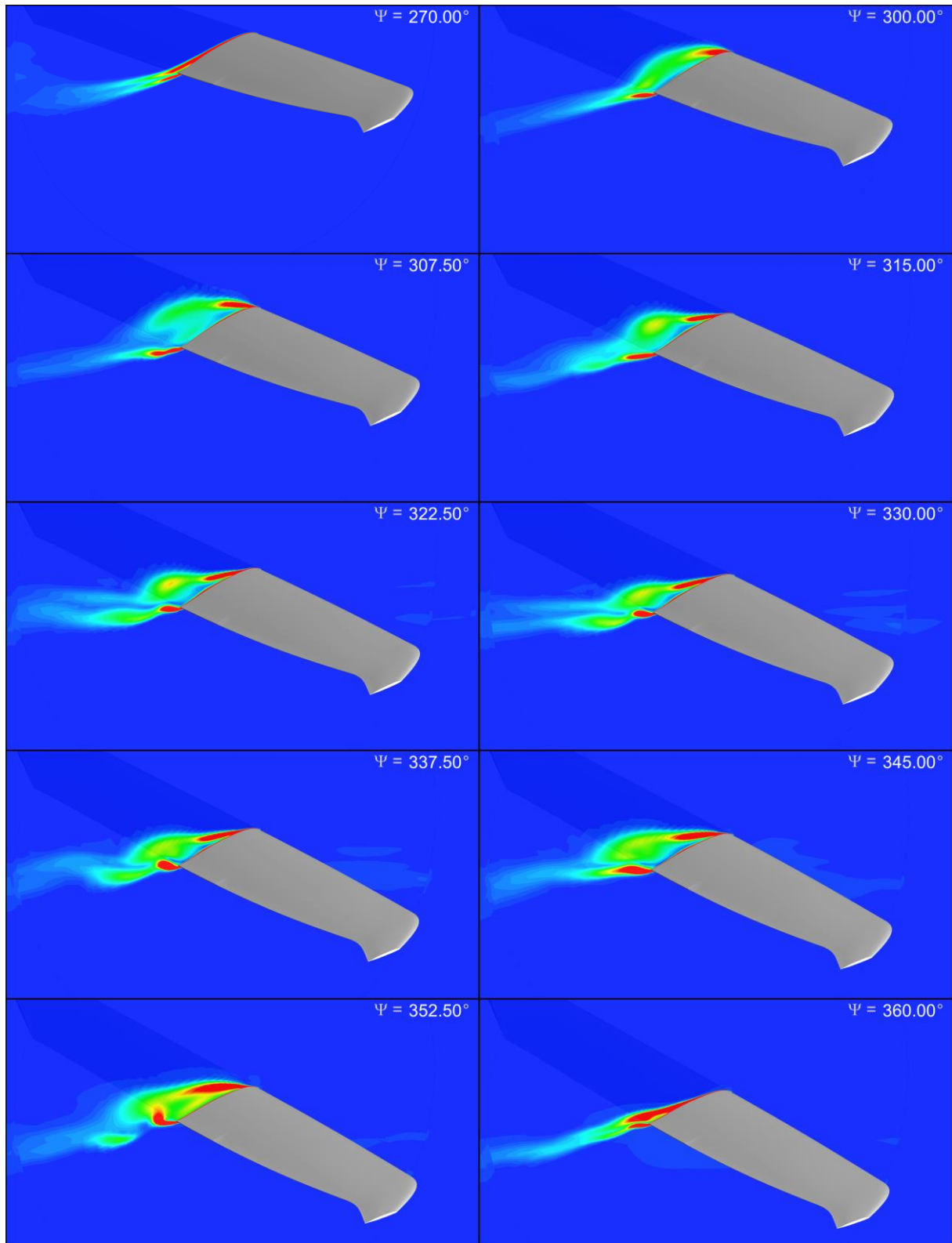


Figure 20. Dynamic-stall phenomenon, visualised in terms of vorticity-magnitude contours, for the case of forward-flight Priority No. 1 configuration "AGF-Sinusoidal" t with moving AGFs. Sequential frames corresponding selected azimuthal positions (Ψ) of the rotor blade.

These differences are especially visible within the range of azimuths corresponding to the dynamic stall ($270^\circ \leq \Psi \leq 360^\circ$) where the torque generated by the blade equipped with AGF is up to 10% lower than the torque generated by the clean blade.

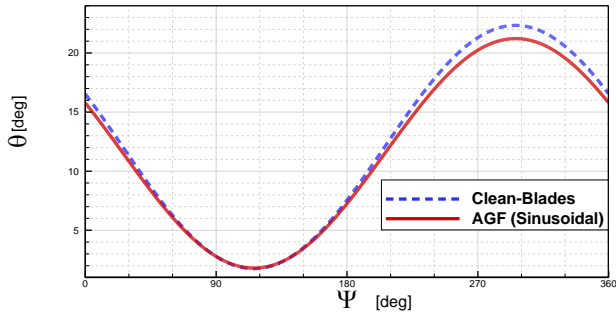


Figure 21. Blade pitch angle (θ) as a function of the blade azimuthal position (Ψ), in trimmed state of the rotor, for Priority No. 1 of forward-flight conditions. Comparison of computational results obtained for "AGF-Sinusoidal" and "Clean Blades" configuration.

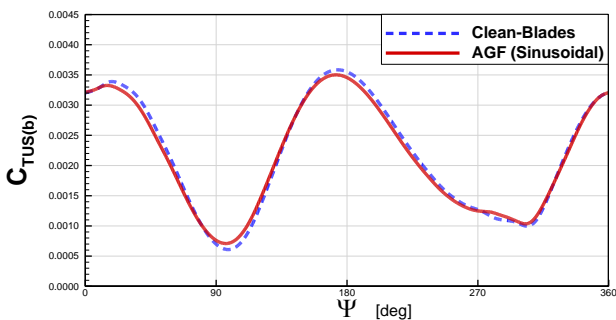


Figure 22. Single-blade thrust coefficient ($C_{TUS(b)}$) as a function of the blade azimuthal position (Ψ), in trimmed state of the rotor, for Priority No. 1 of forward-flight conditions. Comparison of computational results obtained for "AGF-Sinusoidal" and "Clean Blades" configuration.

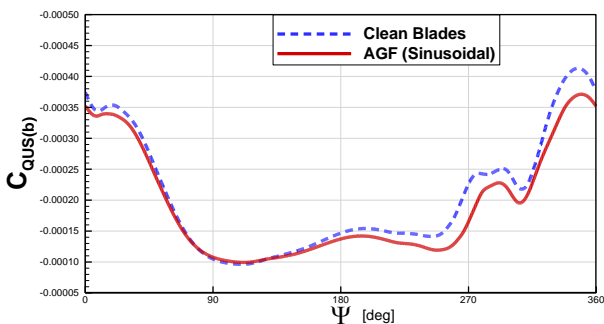


Figure 23. Single-blade torque coefficient ($C_{QUS(b)}$) as a function of the blade azimuthal position (Ψ), in trimmed state of the rotor, for Priority No. 1 of forward-flight conditions. Comparison of computational results obtained for "AGF-Sinusoidal" and "Clean Blades" configuration.

5.2. Computational Studies on the Active Gurney Flap in Hover of Real-Scale Main Rotor

The simulations of hover of the main rotor with blades equipped with the AGFs have been conducted for several hover priorities and for 3 types of AGF kinematics:

- "Clean Blades": AGF fully retracted (reference configuration),
- "1/rev.": 1 cycle of AGF motion per 1 rotor revolution,
- "2/rev.": 2 cycles of AGF motion per 1 rotor revolution.

For each priority, the rotor was trimmed, i.e. the blade-pitch controls were adjusted so as to obtain required thrust and to zero first harmonic components of blade flapping. Based on conducted simulations, it may be concluded that for all considered hover priorities, the configurations with moving AGF ("1/rev." and "2/rev.") have indicated some relative growth of Figure of Merit (ΔFoM), compared to the reference configuration. As shown in Figure 24, the relative growths of Figure of Merit for both configurations with oscillating AGFs are similar to each other for the same values of thrust coefficient (C_{TUS}). In the discussed rotor-hover simulations, the maximum ΔFoM reached approximately 1.5%. The maximum was reached at maximum values of the rotor thrust coefficient.

For the "Clean Blades" and "2/rev." configurations there was no need to set non-zero cyclic pitch of blades to zero first harmonics of blade flapping. However, for the configuration "1/rev.", the fulfilment of "zero-flapping" requirement needed to set commanded cyclic pitch of the blade, which amplitude was of order $0.2 \div 0.3$ degree.

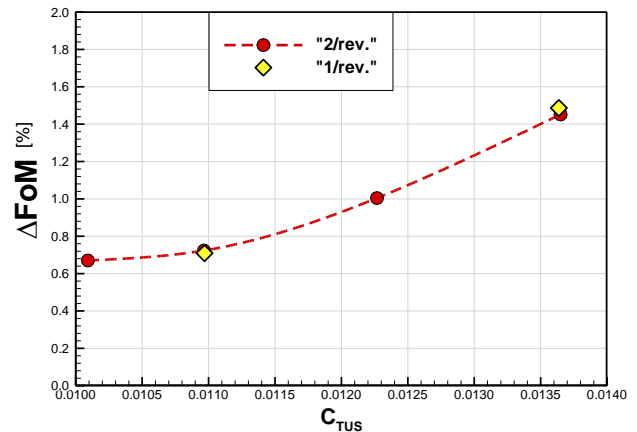


Figure 24. Relative growth of Figure of Merit (ΔFoM) vs. Thrust Coefficient (C_{TUS}) in hover for two configurations of main rotor with oscillating AGF: "1/rev." and "2/rev."

6. CONCLUSIONS

- Application of the AGF technology on the main-rotor blades in forward flight of the helicopter may lead to significant improvement of the performance. The most favourable state of helicopter flight, where benefits resulting from application of the AGF are expected to be most noticeable, is a fast flight at higher values of the rotor thrust coefficient, when the retreating-blade dynamic-stall phenomenon occurs.
- In computational simulations, conducted at higher values of the rotor thrust coefficient, in presence of the retreating-blade dynamic stall, the application of AGF usually led to certain performance improvement, up to 7.3% of relative growth of Power Loading (the ratio: thrust to power) of the rotor. These benefits for both the Active-Gurney-Flap and Passive-Gurney-Flap configurations were similar.
- In computational simulations, conducted at lower values of the rotor thrust coefficient, when the dynamic stall did not occur, the rotor configurations with moving AGFs, compared to the reference configuration (rotor with clean blades), indicated certain slight power penalty. In case of the Passive-Gurney-Flap configuration this penalty was significant, even more than 10% of power losses.
- Optimised ramp schedule of AGF kinematics probably might improve the rotor performance in forward flight, compared to the sinusoidal schedule.
- In certain conditions, the activation of moving AGF on the rotor blades, may lead to performance improvement also in hover of the helicopter. Based on conducted computational simulations, it may be concluded, that the Figure of Merit of the rotor with implemented the AGF technology, may be increased of up to 1.5% (for higher values of the rotor thrust coefficient), compared to the rotor with clean blades. In hover, instead of "1 AGF cycle per 1 rotor revolution" schedule of AGF motion, the more favourable schedule seems to be: "2 AGF cycles per 1 rotor revolution". This is because the later schedule, on the contrary to the former, does not need to set non-zero cyclic pitch of the rotor blades so as to zero the first harmonics of the blade flapping.

SYMBOLS

C	blade chord
C_L	lift coefficient
C_m	pitching moment coefficient
C_{QUS}	torque coefficient (US convention)
$C_{QUS(b)}$	torque coefficient of a single blade
C_{TUS}	thrust coefficient (US convention)
$C_{TUS(b)}$	thrust coefficient of a single blade
h_{agf}	momentary height of AGF
M	Mach number
Q	criterion; $Q = \frac{1}{2} (\omega ^2 - s ^2)$ s-symmetric, ω - antisymmetric components of flow-velocity gradient matrix
P	power
PL	power loading; $PL = T / P$
Re	Reynolds number
t	time
T	period of rotor rotation
V	velocity
α	angle of attack
β	blade-flap angle
ζ	blade-lag angle
σ	rotor solidity
θ	blade-pitch angle
θ_0	collective component of blade-pitch control
θ_s, θ_c	cyclic components of blade-pitch control
ΔP	power-reduction coefficient
ΔFoM	relative growth Figure of Merit
Ψ	azimuthal position of rotor blade: advancing blade: $\Psi = 90deg$ retreating blade: $\Psi = 270deg$

ACRONYMS

AGF	Active Gurney Flap
AoA	angle of attack
CFD	Computational Fluid Dynamic
FoM	Figure of Merit
PGF	Passive (fixed) Gurney Flap
PIV	Particle Image Velocimetry
WTT	Wind Tunnel Tests

ACKNOWLEDGEMENTS

The research leading to these results was financed by the European Union's Seventh Framework Programme (FP7/2007-2013) for the Clean Sky Joint Technology Initiative under grant agreement No.CSJ-GA-2013-619627 and by the Ministry of Science of Poland from funds directed to supporting scientific research, under agreement No.3129/CLEANSKY/2014/2.

Computational support was obtained from University of Warsaw Interdisciplinary Centre for Mathematical and Computational Modelling, in the Computational Grant No.G52-4.

REFERENCES

- [1] ANSYS, Inc., ANSYS FLUENT User's Guide. Release 14.5. Available from: <http://www.ansys.com>.
- [2] Brewer P.R., Raval, R.R., Shorcott, S., Active gurney flap, Patent: EP 2514667 A1, 2012, www.google.co.in/patents/EP2514667A1
- [3] Hairer, Ernst; Norsett, Syvert Paul; Wanner, Gerhard (1993), Solving ordinary differential equations I: Nonstiff problems (2nd ed.), Berlin, Springer Verlag, ISBN 978-3-540-56670-0.
- [4] Gibertini G., Zanotti A., New Technique Implementation in GVPM, Deliverable Report of CleanSky Project GUM, GUM/WP2/D2.3, 2015.
- [5] Kinzel M.P., Maughmer M.D., Duque E.P.N, Numerical Investigation on the Aerodynamics of Oscillating Airfoils with Deployable Gurney Flaps, AIAA Journal Vol.48, No.7, July 2010.
- [6] Leishman G., J., Principles of Helicopter Aerodynamics, Cambridge University Press, 24.04.2006 – 826.
- [7] Stalewski, W., Rotorcraft Applications of Active Gurney Flap Investigated within the Clean-Sky Project COMROTAG, in 41st European Rotorcraft Forum 2015 Proceedings, Volume1. pp. 336-348.
- [8] Stalewski, W., Flow Control on Helicopter-Rotor Blades via Active Gurney Flap, Proceedings of the 30th ICAS Congress of the International Council of the Aeronautical Sciences, ICAS, Daejeon, Korea, 25-30 September, 2016. ICAS 2016 CD-ROM Proceedings.
- [9] Wang J.J., Li Y.C., Choi K.S., Gurney flap - Life enhancement, mechanisms and applications, Progress in Aerospace Sciences 44 (2008), pp.22-47.

Copyright Statement

The authors confirm that they, and/or their company or organization, hold copyright on all of the original material included in this paper. The authors also confirm that they have obtained permission, from the copyright holder of any third party material included in this paper, to publish it as part of their paper. The authors confirm that they give permission, or have obtained permission from the copyright holder of this paper, for the publication and distribution of this paper as part of the ERF proceedings or as individual offprints from the proceedings and for inclusion in a freely accessible web based repository.